Probing electrical transport, electron interference, and quantum size effects at surfaces with STM/STS

by Ph. Avouris I.-W. Lyo Y. Hasegawa

We use scanning tunneling microscopy (STM) and spectroscopy (STS) to probe electrical transport through the dangling-bond surface states of semiconductors and electron scattering and electron confinement effects in metal surface states. Specifically, we use point contacts between the STM tip and the sample to show the existence of surface electrical transport in Si(111)-7×7. Point contacts to silicon islands provide further support for the existence of the surface transport channel and illustrate the role played by carrier scattering at the boundaries of the nanostructure in electrical transport. In contrast to the silicon case, electrons in Shockley-type metal surface states act like a quasi-two-dimensional freeelectron gas (2DFEG). This 2DFEG is scattered

by steps, adsorbates, and defects, and the interference between incident and reflected electron waves leads to an oscillatory local density of states (LDOS). This LDOS is imaged in STM spectroscopic maps, and analysis of the oscillations provides novel information regarding electron scattering by individual surface features. Steps are found to act as barriers for surface electrons, and this property is utilized to confine them and form structures of lower dimensionality. Quasi-1D structures (quantum wires) are generated at narrow terraces of stepped surfaces, while small metal islands behave as 0D structures (quantum dots). Confined states with discrete spectra are observed even at 300 K, and their probability distributions are imaged.

Copyright 1995 by International Business Machines Corporation. Copying in printed form for private use is permitted without payment of royalty provided that (1) each reproduction is done without alteration and (2) the Journal reference and IBM copyright notice are included on the first page. The title and abstract, but no other portions, of this paper may be copied or distributed royalty free without further permission by computer-based and other information-service systems. Permission to republish any other portion of this paper must be obtained from the Editor.

0018-8646/95/\$3.00 © 1995 IBM

1. Introduction

Since its development by Binnig and Rohrer [1], scanning tunneling microscopy (STM) and its spectroscopic version (STS) continue to find new applications. Currently, they are widely used to study, with atomic resolution, metals, semiconductors, superconductors, molecular and biological systems, and adsorbed layers [2]. Here we present two new applications of STM/STS in the study of two- and lower-dimensional electron systems involving electrons in surface states of semiconductors and metals. We first employ STM tip-sample point contacts to explore the possibility of electron transport involving the danglingbond surface states of Si(111)-7×7, and the electrical properties of model nanostructures. We then take advantage of the wave character of the electron and use electron interference effects and surface-state spectroscopy to study the interaction of the quasi-two-dimensional freeelectron gas (2DFEG) formed by the Shockley surface states of Au(111) and Ag(111) surfaces, with individual surface steps and adsorbed or embedded foreign atoms. We use the fact that surface steps act as barriers for electrons to confine them, form lower-dimensionality structures, and observe quantum size effects at room temperature.

The Si(111)-7×7 surface has long been a puzzle for surface scientists. Its complex atomic structure has been the subject of numerous investigations and was finally determined by electron diffraction experiments [3]. However, STM was also crucial in the elucidation of its atomic structure [1]. The electronic structure of Si(111)-7×7 is also intriguing, and has attracted significant attention. Photoemission [4] and inverse-photoemission [5] spectroscopies indicate that the surface, so-called Si adatom layer has a metallic character, and STS spectra [6] corroborate this conclusion. However, the dangling bonds of the adatom layer are spaced far apart (~7 Å), and no dispersion is observed by angle-resolved photoemission [4], a fact that indicates a very weak interaction between the dangling bonds. Attempts at direct measurement of electrical transport involving these states have been unsuccessful [7]. However, the anomalous broadening of the quasi-elastic peak observed in electron energy loss studies of Si(111)-7×7 has been interpreted as indicating the presence of ac surface conductivity [8].

Here we report on our efforts to measure electrical transport directly through the dangling-bond states of the 7×7 surface structure. In our approach to this problem, we decrease the importance of bulk transport by using rectifying, not ohmic, metal–semiconductor contacts, and by increasing the spreading resistance $[\rho \sim 1/(\text{radius of contact area})]$ through the use of the ultrasharp STM tip. Surface and bulk contributions to electrical transport are then resolved by exposing the sample to gases which are

known to react chemically with the surface dangling bonds and thus affect surface conduction. In this way, we are able to observe, for the first time, conduction involving dangling-bond surface states.

We also use STM tip-sample contacts to electrically address individual nanostructures. While there is considerable interest in the electrical properties and quantum size effects occurring in nanostructures, there has not been a way to establish proper electrical contacts with such structures. The ability of the STM to image a set of nanostructures, select a particular one, and electrically address it through a point contact makes the STM an ideal tool for studies of transport through nanostructures.

The behavior of electrons in surface states of metals can be very different from that of electrons in dangling-bond states of semiconductors. Of particular interest are s,p-electrons in the so-called Shockley surface states. In these states, the electrons are confined to the surface region by a projected bulk band-gap on one side and by the vacuum barrier on the other, and the electrons are not strictly confined to the top layer; there is considerable bulk penetration. Most significantly, the electrons are free to move parallel to the surface, forming a quasi-two-dimensional free-electron gas (2DFEG). One complication of this simple picture results from the mixing of bulk and surface states in the vicinity of surface defects. Typical cases of Shockley surface states are provided by the (111) surfaces of the noble metals: Cu, Ag, and Au [9].

In this paper we examine the interaction of the 2DFEG present at the (111) surfaces of Au and Ag with features such as surface steps or adsorbed atoms. Because of particle-wave duality, an electron acting as a wave can interfere with itself. A surface-state electron incident on one of the above obstacles is partially reflected. The reflected and the incident wave then interfere to give an oscillatory local density of states [LDOS (E, r)] in the vicinity of the obstacle. The first attempt to study such electron interference effects with STM was made by Jaklevic and co-workers [10]. More recently, two IBM groups [11, 12] were able to image the LDOS oscillations directly with STM and STS.

Here we present results illustrating the reflection and interference induced by steps and adsorbed atoms at Au(111) and Ag(111) surfaces. We investigate the spatial extent of the electron-step and electron-adsorbate interactions by studying the surface-state spectrum as a function of the distance from steps and adsorbates. Since surface steps act as barriers for surface electrons, we have used narrow terraces and metal islands to confine these electrons and form low-dimensionality structures. With the STM we are able to image the probability distributions of the particle-in-a-box-like states formed and obtain their discrete spectra. Because of the ultrasmall size of these

structures, we can observe quantum size effects even at room temperature.

2. Experimental section

All experiments were carried out at room temperature in ultrahigh vacuum (UHV) (base pressure 2×10^{-10} torr). The Si(111) and Si(100) samples were commercial, polished wafers (1 Ω -cm P-doped and 0.1 Ω -cm B-doped). The native oxide was removed either by thermal flashing or by HF etching followed by hydrogen thermal desorption. Si epitaxial islands were grown by evaporating silicon on a Si(111) substrate held at 400°C. The Au(111) samples were prepared *in situ* by evaporation of the metals on cleaved mica at room temperature, and subsequent annealing at $\sim 600^{\circ}$ C. W tips were used for imaging, while both W and Al tips were used in point-contact spectroscopy (*I-V* measurements). Mo clips and W blocks on the front and back sides of the sample were used to make electrical contact and keep the sample in place.

The STM and the scanning tunneling spectroscopy (STS) setups have been described elsewhere [13]. Control of the STM tip motion is accomplished by adding D/A-converter voltages to the z-piezoelectric voltage. *I-V* measurements as a function of tip-surface distance are performed by disabling the feedback loop, displacing the tip, typically by 0.1 Å, and ramping the bias voltage; then the sequence is repeated. *I-V* data are continuously collected both as the tip approaches the surface and as it is retracted. In this way, we can monitor any changes in the electronic structure of the tip or sample.

3. Results and discussion

• The STM as a probe of electrical transport

Electrical properties of nanometer-scale contacts In Figure 1, the differential conductance (dI/dV) at V=0 is plotted as a function of tip-sample distance for three different materials: a polycrystalline gold sample, and single-crystal Si(111)-7×7 and Si(100)-2×1 samples. Zero tip displacement corresponds to the tip position during normal tunneling operation, while tip displacement of about 6 Å leads to tip-sample contact.

As Figure 1 shows, when gentle contact is established with the gold sample, the value of the conductance is very close to $2e^2/h$. When the tip is further pressed against the sample, the value of the conductance increases. A conductance of $2e^2/h$ is characteristic of conduction through a single ideal transport channel [14]; moreover, it suggests a contact area of atomic dimensions. This can be understood by considering the lateral confinement of the electrons in the constriction formed by the contact of the sharp metal tip and the sample. This lateral confinement of the electrons should lead to the formation of discrete

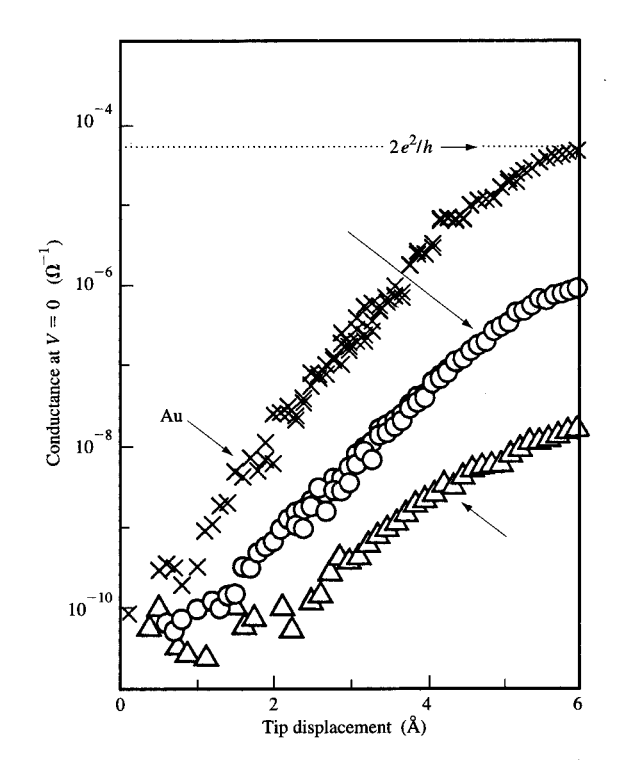


Figure :

Conductance at V=0 plotted as a function of the displacement of the tip from the tunneling position. Measurements are shown for three samples: polycrystalline Au(111), a Si(111)-7×7 surface, and a Si(100)-2×1 surface.

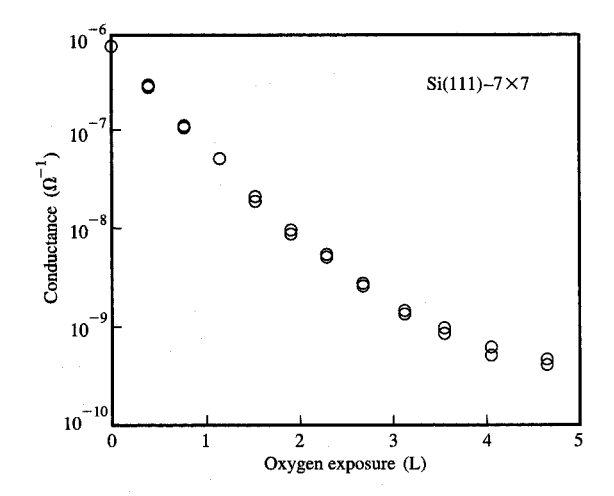
quantum levels (modes) which are analogous to the modes of an electron waveguide. Electrons occupy these discrete states and are free to move along the constriction direction. The conductance *G* is given by the two-terminal Landauer equation [14]

$$G = \frac{2e^2}{h} \sum_{n=1}^{N} T_n(E_{\rm F}), \tag{1}$$

where T_n is the transmission of the *n*th mode. If no backscattering occurs,

$$\sum_{n=1}^{N} T_n(E_{\rm F}) = N,$$

the number of occupied modes. We can estimate this number for an atomic-scale constriction by noting that if W is the width of the constriction, the resulting quantum modes should satisfy the relation $W = n(\pi/k)$, where k is their wavenumber. Now the number of occupied modes N is given by n when k is taken to be k_F , i.e.,



Dependence of the conductance measured with the tip in contact with a Si(111)-7 \times 7 surface as a function of exposure to O₂.

 $N = \text{Int}(k_{\rm F}W/\pi)$. Thus, for typical values of W = 2.5 Å, $k_{\rm F} = 1.5 \text{ Å}^{-1}$, N is 1, and the expected conductance is $2e^2/h$, as found here. Although the above discussion is somewhat simplistic, it does give credence to the assertion that atomic-scale contacts can be produced with the STM.

While, as we saw, the electrical properties of the tip contact to the metal sample can be understood in terms of constriction resistance, the properties of the contacts to the two silicon surfaces behave in drastically different manners. The conductance values are respectively two and four orders of magnitude lower than that of gold for Si(111)-7×7 and Si(100)-2×1. The contact conductance of $Si(111)-7\times7$ is different from that of $Si(111)-2\times1$, even when the two samples have the same bulk conductivity. Moreover, the conductance is independent of the doping; i.e., both p- and n-doped samples have the same contact conductance. These observations suggest the involvement of a surface transport channel. This notion is further supported by the fact that the observed conductances are much larger than the value expected (less than $10^{-12} \Omega^{-1}$) if transport were to be limited by the Schottky barrier that should form at the tip (tungsten)-silicon interface [15].

Surface electrical transport on Si(111)

The involvement of the surface in the electrical transport was confirmed in an experiment in which, after the electrical contact was formed, the Si(111) surface was exposed to gases that react with the surface dangling-bond states and the change in conductance was measured [16]. Figure 2 shows the behavior of a W-Si(111) contact after

exposure to O_2 . It is seen that after an exposure of ~ 5 L (1 L = 10^{-8} torr.s) of O_2 , the conductance decreased by about three orders of magnitude. The same reduction was observed when an aluminum tip was used.

Information about the electronic structure of the point contact can be obtained by the analysis of the I-V characteristics of the contact. Figure 3 shows the characteristics of a \sim 5-nm-diameter W-Si(111)-7×7 contact (the diameter was determined by breaking the adhesive contact and imaging the affected area of the

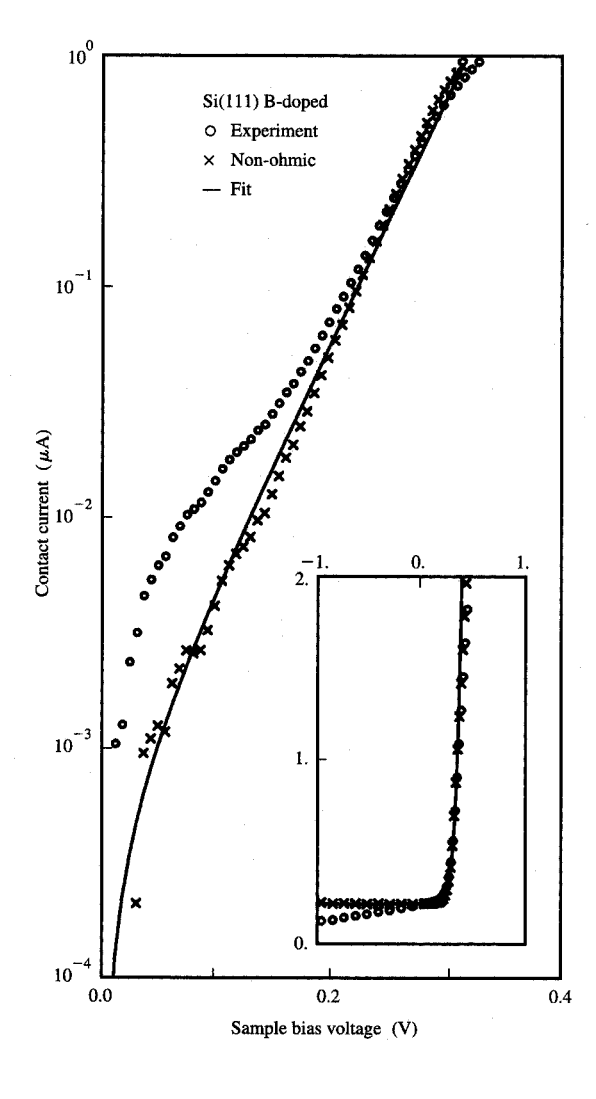


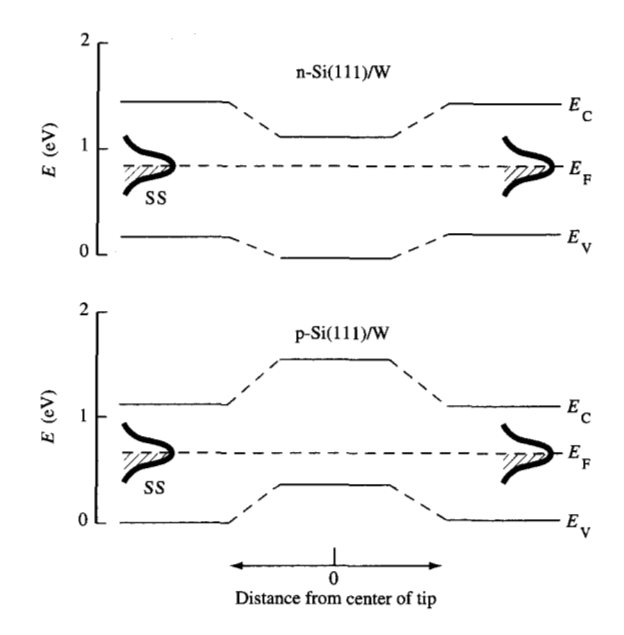
Figure 3

Current vs. sample bias voltage of a point contact between a W tip and a Si(111)–7×7 (B-doped) sample. The experimental data are shown as open circles, while \times 's give the current after the subtraction of the ohmic component. The solid line gives the fit to the Schottky equation. Inset: *I-V* curves of the point contact.

surface). The I-V values show strong rectification behavior, with the contact acting as a nanometer Schottky diode. For reverse bias we observe an ohmic "leakage" current. We find that it is this linear component which is most sensitive to O₂ exposure, and thus can be attributed to the surface transport channel. After subtraction of this "leakage" current, the I-V data can be fitted to the Schottky equation $J = J_s(\exp \alpha V/kT - 1)$ to obtain the saturation current density J_s , and from it the Schottky barrier, $\phi_{SR} = (kT/q) \ln[(A^{**}T^2)/J_s]$, can be extracted using a typical value for the Richardson constant A** of 120 A/cm²/K² [15]. In this way, we can determine the relation of the valence and conduction bands at the contact area to the corresponding bands in the adjacent area. The results are shown in Figure 4. We see that there are barriers to the flow of electrons from the conduction band of the contact area to the surrounding area. Similarly, a barrier exists to inhibit the flow of holes out of the valence band of the contact area. On the other hand, the danglingbond surface states overlap and pin the Fermi level, and, provided that there is interaction between the dangling bonds, current could flow through this channel.

The experimental observations presented above prove the existence of a surface transport channel, and, moreover, allow identification of the nature of this channel. In principle, there are two possibilities: One involves transport through the dangling-bond surface state, while the other involves a space-charge layer present due to surface band-bending. To our knowledge, previous work on semiconductor surface transport has always implicated transport involving the space-charge layer. The evidence presented here, however, is consistent with transport via the surface state. Specifically, the finding that the contact resistance is independent of the bulk doping cannot be reconciled with a transport mechanism involving the spacecharge layer. Moreover, the very large (10³×) reduction in conductance upon O₂ exposure would require a very strongly accumulated or inverted space-charge layer to be present at the surface of $Si(111)-7\times7$. However, it is well established that the Fermi level is pinned by the surface states at 0.6 eV above the valence band maximum [17], leading to an electron depletion layer for n-type 7×7 surface, and a hole depletion layer for p-type 7×7 surface. Finally, as we discussed above, the electronic structure shown in Figure 4 provides another reason why transport through the surface state should be important. More evidence is provided when we next consider the behavior of tip point contacts to model nanostructures.

As a simple model of a nanostructure whose electrical properties we want to determine by tip-sample point contacts, we have selected small 7×7 Si epitaxial bilayer islands grown on Si(111). These islands are formed in various sizes when Si is deposited on Si(111). The advantage of these epitaxial structures is that the coupling

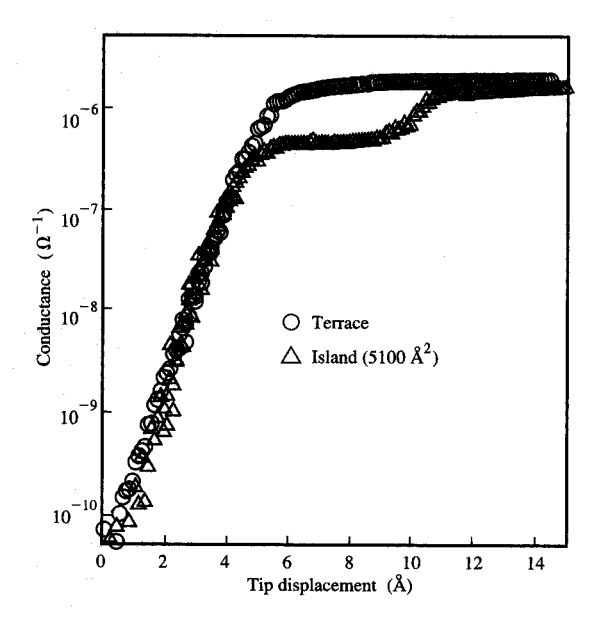


Holling

Diagrams showing the energies of the top of the valence band and the bottom of the conduction band of an n- and a p-doped sample in contact with a W tip. The area of the surface in contact with the W tip is depicted in the middle of the diagram. The surface states (dangling bonds) in the surrounding clean 7×7 surface pin the Fermi level.

of their surface layer to the bulk is the same as the surface-layer-bulk coupling on the surrounding terrace. The experiment then consists of measuring and comparing the conductances obtained by tip point contact on top of an island and on the adjacent terrace. The two conductances measured in this way are found to be different. Although the exact numerical value of the difference varies somewhat from experiment to experiment, the conductance of the island is always smaller. The results of such an experiment are shown in Figure 5. It is seen that the conductance of the island measured by the initial tip contact is smaller, but continuing to press the tip against the sample with the z-piezoelectric transducer increases the conductance until it reaches that of the terrace.

Given that coupling to the bulk is the same for both the island and the substrate, the above findings can be explained by again invoking the presence of transport through the dangling-bond surface state. One would then expect that the steps surrounding the island would act as barriers to transport, scattering the carriers and leading to a reduced conductance [16]. When the tip is pressed against the island, however, the contact area increases,



Conductance at V = 0 plotted as a function of displacement of the STM tip from the tunneling position toward contact, measured on an epitaxial Si(111) island and on the surrounding Si(111) terrace.

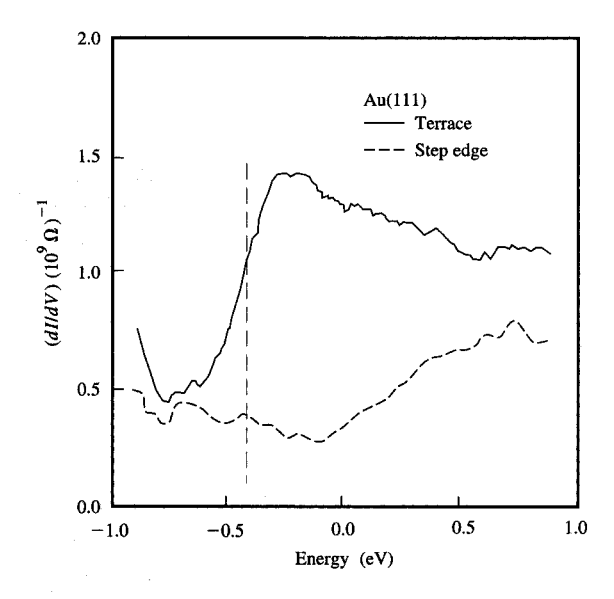


Figure 6

Tunneling spectra obtained over a terrace site of a Au(111) surface (full line) and directly over a step of the same surface (dashed line).

and at some point contact with the surrounding substrate is achieved and the conductance becomes the same as for direct contact to the substrate.

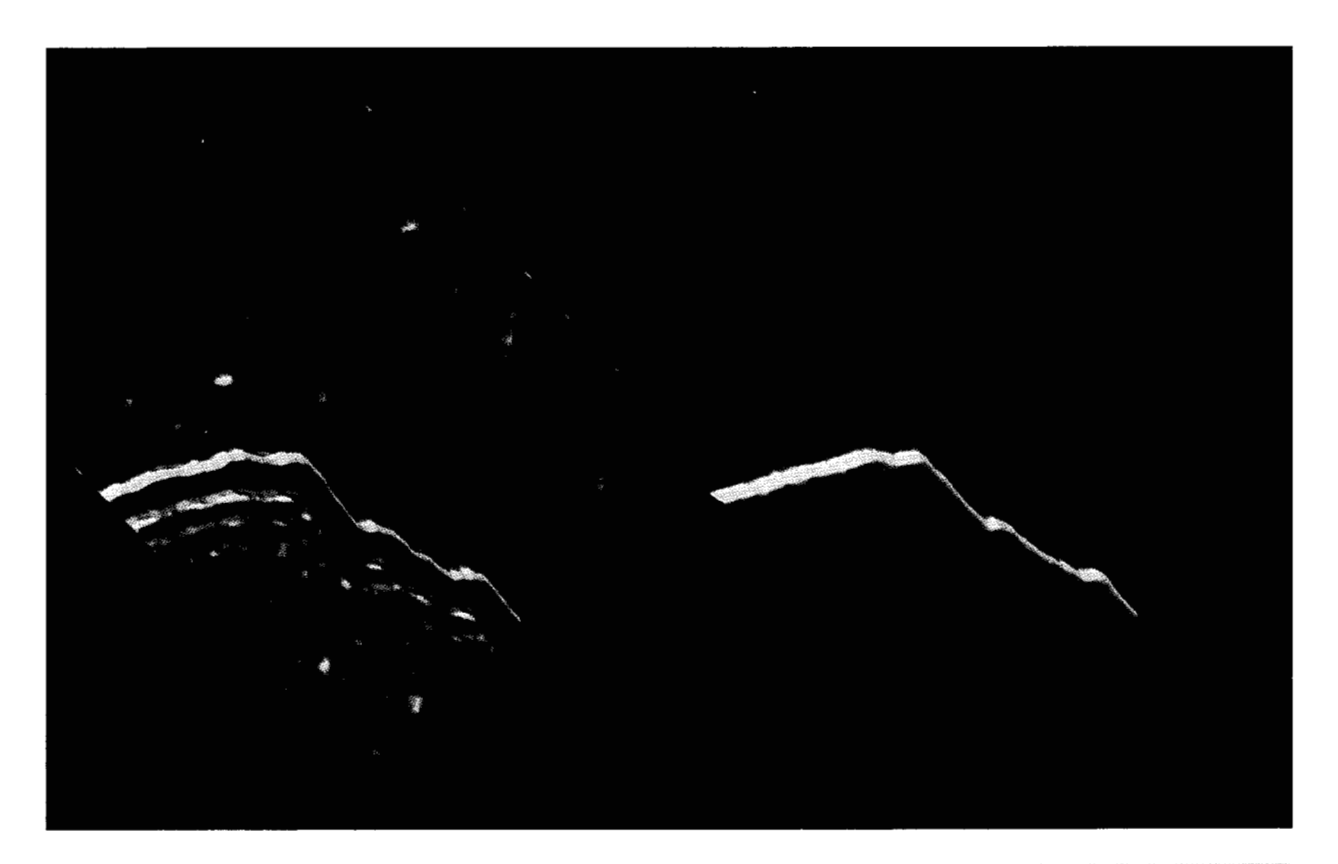
While the carrier-scattering processes at the boundaries of the island are studied indirectly from their effect on the value of the contact conductance, we see next that electron-scattering processes at metal steps can be studied more directly by observing electron interference patterns.

Scattering and confinement of electrons at metal surfaces

Scattering of surface-state electrons by steps and point defects

Electrons in Shockley surface states of metals provide a new quasi-two-dimensional electron gas (2DFEG) system of higher electron density than those provided by inversion layers in semiconductors [18] or semiconductor heterostructure interfaces [19]. It is not, however, obvious how to study such a system with STM/STS. A true 2D electron system has a constant density of states (DOS), so STS should not be of much help. However, it is not the 2DFEG itself that is the main interest here, but rather its interaction with scattering potentials produced by adsorbed or embedded atoms or structural features such as surface steps [20]. As we see below, these types of interactions can be studied by STS.

A typical example of Shockley surface states is provided by the s,p-electrons of the (111) surfaces of the noble metals, Cu, Ag, and Au [9]. The surface-state wavefunction decays exponentially at both the vacuum and bulk sides of the surface because of the vacuum barrier and a projected bulk $L_2' - L_1$ band-gap, respectively. In Figure 6 we show STS spectra of a Au(111) surface near the onset (E_0) of its surface state. The full line gives the spectrum obtained over a terrace site of the Au(111) surface and clearly shows the onset of the surface state at about 0.4 eV below $E_{\rm F}$. When the tip is placed directly over a surface step, however, the characteristic onset of the surface state is absent. We observe an analogous behavior near point defects and adsorbates. The fact that the surface state is not observed in the vicinity of the above surface features can be described by considering the step or adsorbate to act as an electron barrier, e.g., a potential energy wall or well. The picture is analogous to that used to model electrical resistivity due to point and extended defects [21]. The de Broglie wavelength of the electrons at the noble metal surfaces is significantly larger than that in the bulk of the materials. At the Fermi energy, the surface electron wavelengths for Cu(111), Ag(111), and Au(111) are 29 Å, 49 Å, and 36 Å, respectively [9]. When an electron wave is incident on a step or defect, it is scattered. The reflected part of the wave can then interfere with the incident part, resulting in an oscillatory local



Floure 7

Top: STM image of a Au(111) surface showing two terraces (sample bias = -1 V). Bottom: Spectroscopic image at $V_S = +0.15$ V, constructed from *I-V* curves obtained at 3-Å intervals over the same area shown in the STM image. From Reference [11a], reproduced with permission.

density of states (LDOS), i.e., a standing wave in the vicinity of the step [11, 12]. In the case of two-dimensional scattering, the resulting LDOS oscillations should, in the absence of other dephasing processes, decay slowly as a function of the distance x away from the step. If we assume that the scattering potential can be modeled by a hard wall, then the resulting local density of states $\rho(E,x)$ is given simply by

$$\rho(E, x) \propto 1 - J_0(2k_{\parallel}x), \tag{2}$$

where J_0 is the zeroth-order Bessel function, and k_{\parallel} is the wavenumber parallel to the surface, i.e., $k_{\parallel} = (k_x^2 + k_y^2)^{1/2}$. The decay of the oscillations with distance x from the step can be seen from the asymptotic form of the Bessel function:

$$J_0(2k_{\parallel}x) = \left(\frac{1}{\pi k_{\parallel}x}\right)^{1/2} \cos\left(2k_{\parallel}x - \frac{1}{4}\pi\right). \tag{3}$$

In contrast to steps, scattering of the long-wavelength surface waves by point defects of atomic dimensions is expected to lead to isotropic scattering, giving rise to circular waves surrounding the point defect. Within the s-wave approximation, $\rho(E, r)$ is given [11] by

$$\rho(E, r) \propto 1 + \frac{2}{\pi k_{\parallel} r} \left[\cos^2 \left(k_{\parallel} r - \frac{\pi}{4} + \eta_0 \right) - \cos^2 \left(k_{\parallel} r - \frac{\pi}{4} \right) \right], \quad (4)$$

where η_0 is the s-wave phase shift.

In addition to elastic scattering, another possible scattering channel involves the scattering of electrons in surface states to bulk states. This becomes possible because, while surface and bulk states are orthogonal to each other at a perfect surface, defects allow such states to mix in their vicinity [22, 23]. This scattering channel reduces the amplitude of the elastically reflected wave, and thus the intensity of the LDOS oscillations, and modifies the observed phase shifts [24].

Examples of LDOS oscillations observed at Au(111) and Ag(111) surfaces at room temperature are shown in Figures 7 and 8. Figure 7(a) is an STM image of a Au(111) surface

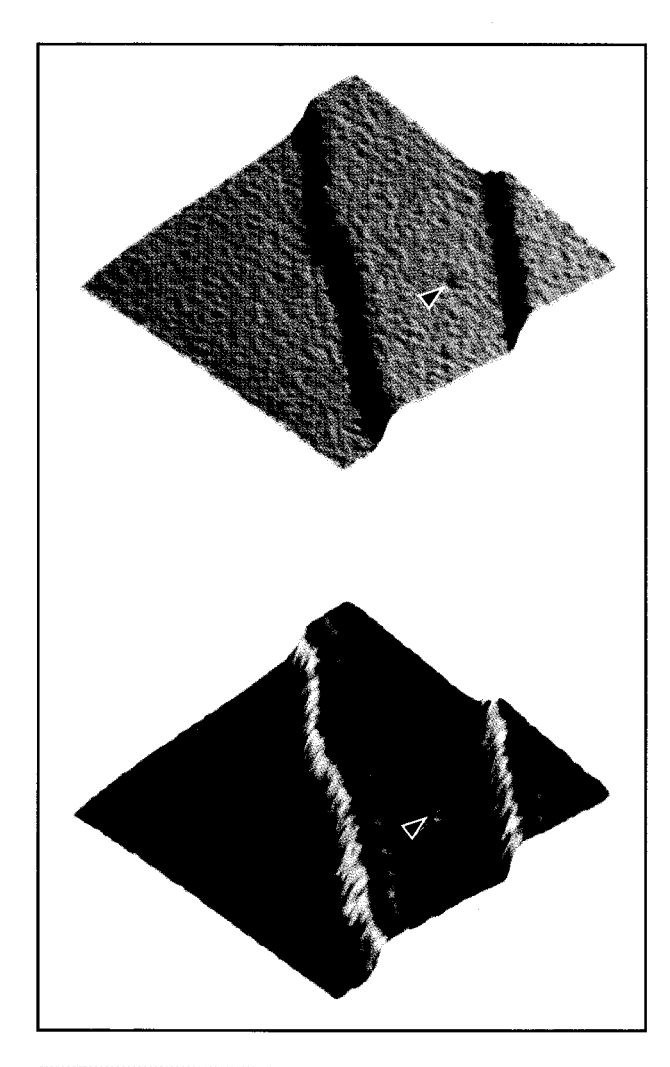
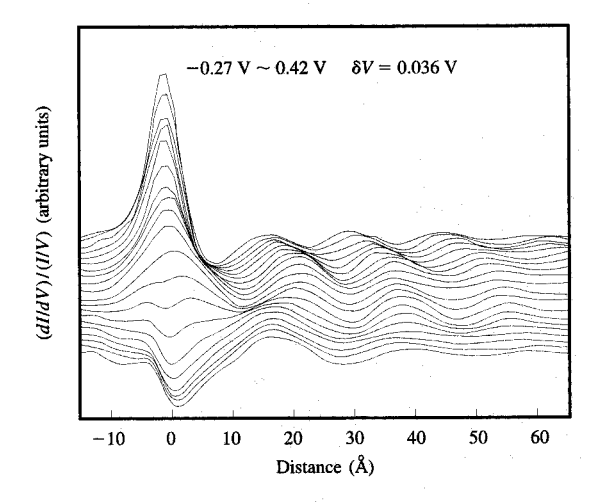


Figure :

Top: STM image of a 32×32 -nm² Ag(111) surface showing areas of three terraces ($V_S = +0.17$ V). Bottom: Spectroscopic image of the same area superimposed on the STM image ($V_S = +0.44$ V). The arrow points to an impurity atom. From Reference [11b], reproduced with permission.

showing parts of two terraces obtained at a sample bias of -1 V. A small corrugation (\sim 0.1 Å) due to the $22 \times \sqrt{3}$ reconstruction on the Au(111) surface [25] is observed faintly, particularly on the lower terrace. In addition to the topographic image, we have obtained tunneling spectra at 3-Å intervals over the entire area shown in the image of Figure 7(a). By using these I-V data, spatial images of the derivative dI/dV or (dI/dV)/(I/V) at given voltages can be produced. We refer to such images as spectroscopic maps. Such a map for V = +0.15 V is shown in Figure 7(b). Here, bright contrast indicates a large value of the current derivative. Since the value of dI/dV provides a rough measure of LDOS, we can consider the image of Figure



Напра 9

Laterally averaged (dI/dV)/(I/V) line scans perpendicular to a step on a Au(111) surface as a function of the bias.

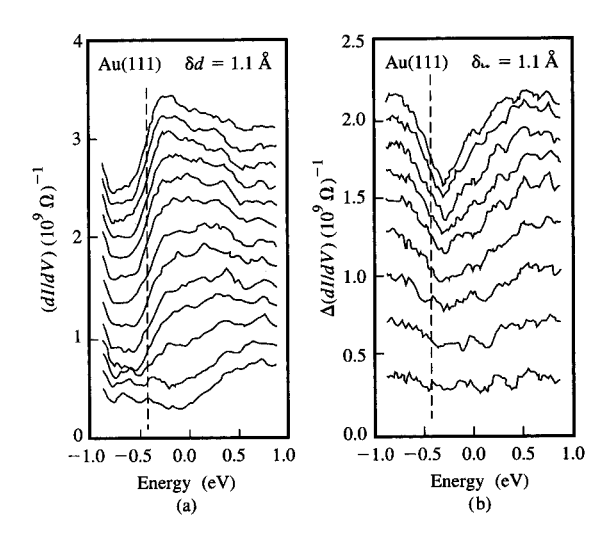
7(b) as a map of the surface LDOS at an energy of about 0.15 eV above $E_{\rm F}$. This image shows a bright line, i.e., high LDOS, right at the step, and behind the step on the upper terrace side are several more bright lines running parallel to the step. The spacing between the lines is about 16 Å. These observations are in agreement with an electron interference origin of the observed oscillations. The distance between two antinodes of the interference pattern should equal half the electron wavelength, which, according to the known dispersion of the Au(111) surface state [9], should be about 31 Å at 0.15 eV above $E_{\rm E}$. In Figure 8(a) we show an STM topograph of a Ag(111) surface at +0.17 V, while in Figure 8(b) we give the corresponding spectroscopic map (superimposed on the STM topograph) obtained at +0.44 V. This map shows not only the oscillations associated with the steps, but also scattering by an impurity atom which is barely visible as a dark spot (see arrow) in the topographic image of Figure 8(a). As expected, the point defect produces oscillations in the form of concentric rings.

In order to be able to quantify our observations, we utilize STM line scans normal to the direction of the step. To improve the signal-to-noise ratio, these scans are laterally averaged. Figure 9 shows line scans along the $\langle \overline{1} \ \overline{1} \ 2 \rangle$ direction of Au(111) for a range of energies (voltages) from 0.38 eV below $E_{\rm F}$ to 0.45 eV above $E_{\rm F}$. From such line scans we find that the oscillations decay faster than expected from Equations (2) and (3). The intensity decays exponentially with distance x from the step: $I \propto \exp(-x/I_{\rm c})$. This behavior was explained [11] as reflecting the fact that STM does not probe a single

k-level, but rather an electron wave-packet with a Δk_{\parallel} -spread determined by the temperature-dependent energy resolution ΔE . For a parabolic band $\Delta k_{\parallel} = (m^*\Delta E)/(\hbar^2 k_{\parallel})$, with $\Delta E \approx 3.5~k_{\rm B}T$. The coherence length $I_{\rm c}$ is then given by $I_{\rm c} \sim 1/\Delta k_{\parallel}$. The observed $I_{\rm c} \approx 30$ Å is in rough agreement with these expectations [11]. From dI/dV line scans one can also determine the dispersion (E vs. k_{\parallel} relation) of the surface state. Similarly, information on the scattering phase shifts can be obtained by fitting dI/dV scans.

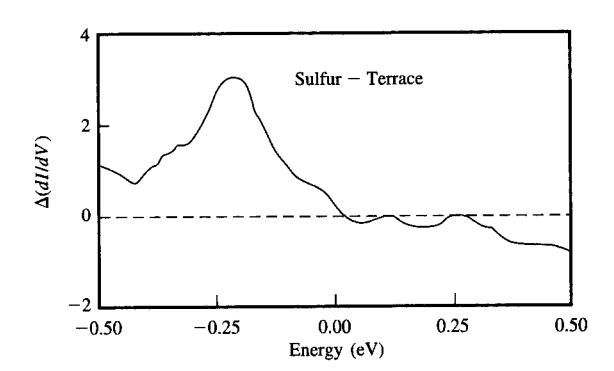
Another approach to the study of the interaction of surface-state electrons with various surface features is provided by the effect of these perturbers on the surfacestate spectra. Since the surface-state spectrum is essentially featureless, we concentrate our attention on the onset region. In Figure 10(a) we show a number of spectra of this region as a function of the distance of the tip from a surface step of a Au(111) surface [26]. The bottom line corresponds to the spectrum obtained directly over the step, and the distance between successive steps is 1.1 Å. Considering the shapes of the spectra, we note that the perturbation of the onset region produced by the step extends more than 10 Å away from it. Moreover, the nature of the spectral modification is very characteristic. In Figure 10(b), we show the difference between the spectra obtained at distances x > 4 Å from the step and that obtained at x = 4 Å. We see that the main effect of the step is to reduce the intensity (i.e., the LDOS) near the onset region of the surface-state band. This is the region that should be most sensitive to the dimensionality of the electronic band. While 3D electron systems have a vanishing DOS at the electronic band origin, 2D systems have a step-function-like DOS at the onset of the band [18]. It is thus plausible that as we approach the surface step, the increasing surface-bulk mixing induced by the step leads to a larger bulk penetration and a 3D-like character for the band. While on a flat perfect terrace the bulk and surface states are orthogonal to each other, the reduction of symmetry near a defect leads to bulk-surface mixing.

Next we consider the scattering of the surface-state electrons by point defects, e.g., foreign atoms. Figure 11 shows the tunneling spectrum over a sulfur atom at a Ag(111) surface. The spectrum shown is the difference between the spectrum (dI/dV vs. E) recorded directly over the impurity and the spectrum obtained over a clean surface site. It shows that this impurity leads to an enhancement in the LDOS below $E_{\rm F}$, with a peak at \sim 0.2 eV and a decrease in LDOS above $E_{\rm F}$ [26]. What is particularly remarkable in the spectrum of Figure 11 is its extremely narrow bandwidth (\sim 200 mV). As we discussed in more detail elsewhere [26], the 3p levels of sulfur are in resonance and can interact with the silver d-band to give a set of $3p_z$ and $3p_{x,y}$ bonding and anti-bonding levels.



Tellife 10

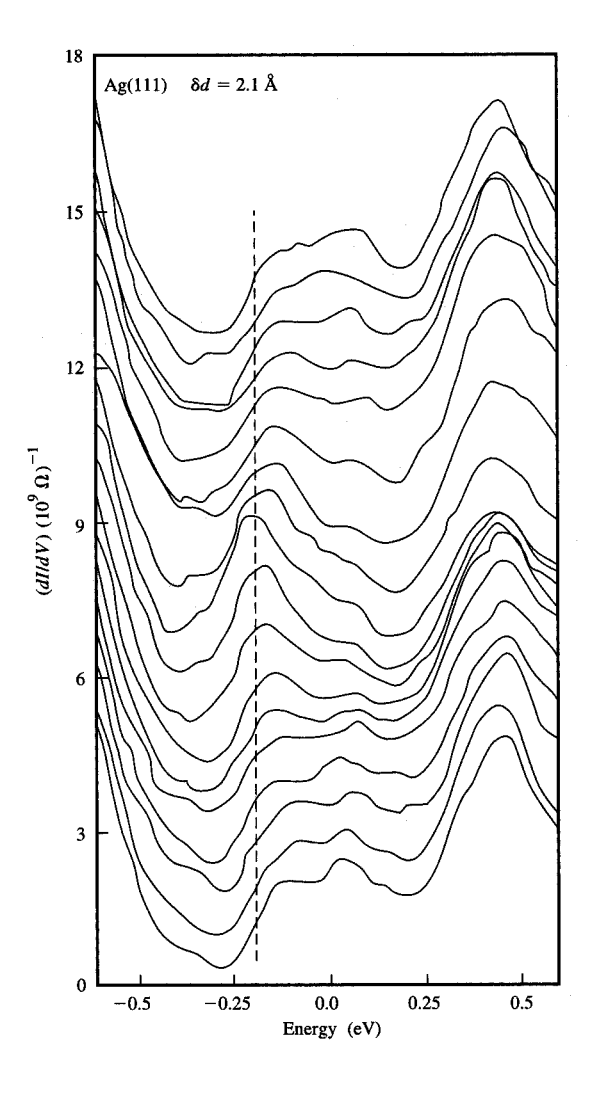
(a) Tunneling spectra of the onset region of the surface state of Au(111) as a function of the distance from a step. The bottom spectrum is taken directly over the step, while the rest are taken at 1.1-Å intervals. (b) Difference between the spectra obtained at distances x > 4 Å from the step and that obtained at x = 4 Å.

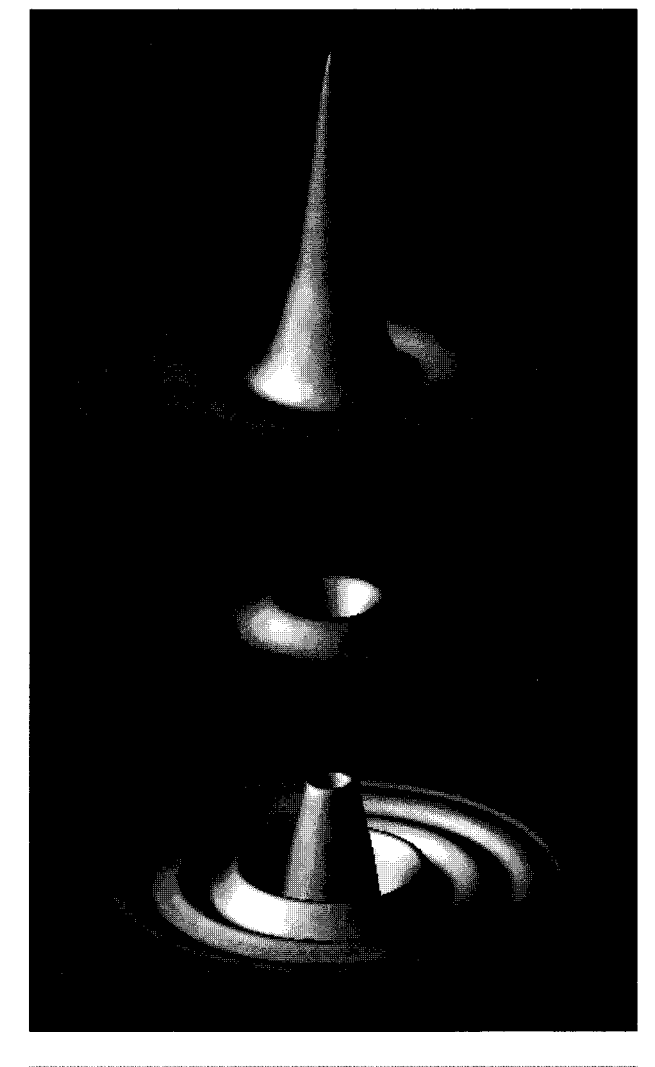


Force

Difference between the tunneling spectrum recorded directly over an impurity atom at a Ag(111) surface and the spectrum obtained over a clean surface site.

These levels further hybridize and are broadened by the interaction with the silver sp-band. The level detected by the STM is the $3p_z$ level that falls at the edge of the Ag sp-gap at the L_2 point of the Brillouin band. The small width results from the low density of bulk states with which hybridization can occur. Other factors leading to narrow widths in STS involve the lack of inhomogeneous





Tunneling spectra of the onset region of the Ag(111) surface as a function of the distance from a sulfur impurity atom. The middle spectrum corresponds to the tip centered over the impurity. The spacing between adjacent spectra is $\sim\!2.1$ Å. The peak at $\sim\!0.4$ eV is tip-related.

broadening and dispersion, since individual, isolated adsorbates are studied.

We again use the onset region of the surface-state spectrum as a measure of the extent of the perturbation by the defect. Figure 12 shows a series of such spectra as a function of the distance from the sulfur atom. As the impurity is approached, we see a progressive reduction of the surface-state spectrum and an increased spectral localization around it. From Figure 12, the range of the perturbation is seen to be at least 15 Å.

Flaure 13

Rotationally averaged dI/dV images of a sulfur atom adsorbed on Ag(111). The sample bias from top to bottom is -0.1 V, +0.1 V, and +0.4 V.

The LDOS oscillations generated by the impurity at room temperature are weak. To increase the signal-to-noise ratio, we generate dI/dV line scans through the impurity and average them rotationally. These averaged line scans are then used to generate the 3D dI/dV images of the sulfur impurity shown in Figure 13. The images correspond to a sample bias of -0.1 V, +0.1 V, and +0.4 V (top to bottom). The oscillations surrounding the sulfur impurity can be described as energy-resolved Friedel oscillations resulting from the screening of the excess charge on the S atom by the surface-state electrons. The scattering and screening descriptions of the oscillations are equivalent. The screening description, however, allows one to obtain more directly information on the net charge on

the adsorbate and thus gain insight into the nature of the chemisorption bond. The S atom in this case forms a closed 3p-shell [26], is negatively charged, and gives rise to a protrusion in the occupied-state image. Inverse-photoemission spectra of S on Cu(100) [27] show that the 3d states are located at much higher energy. This lack of low-energy unoccupied states is responsible for the hole at the origin in the unoccupied-state images of Figure 13. The energy (bias) dependence of the intensity of the oscillations was discussed in Reference [16].

Quantum size effects at metal surfaces: Electron confinement in low-dimensionality structures The 2DFEG system produced by semiconductor heterostructures can be patterned through lithographic techniques or by electric fields to give structures of even lower dimensionality, i.e., 1D structures (quantum wires) and 0D structures (quantum dots). Since, as shown above, steps act as barriers for surface electrons, they can be used to form low-dimensionality structures. For example, one could form quasi-1D structures by creating narrow terraces whose width is of the order of the Fermi wavelength, which in the case of the (111) surfaces of noble metals is a few nanometers. Stepped surfaces with variable terrace width can be produced by cutting a single crystal at a small angle with respect to a low-index crystal plane, or simply by the controlled annealing of thin films. Figure 14 shows such a stepped Au(111) surface produced by annealing, on which 0D-like structures are generated by metal-on-metal evaporation and nucleation to form metal islands. Depending on the conditions (substrate temperature, surface coverage, and annealing), islands with different sizes and shapes can be produced [28]. Both islands and narrow terraces are stable over a wide range of temperature. A different approach has been utilized by Crommie et al. [29], who arranged Fe atoms on Cu(111) at 4 K to form closed structures (quantum corrals) and thus generate confined states.

Narrow terraces produce electron confinement in the direction normal to the step (x-direction), while electron motion parallel to the step (y-direction) is free. Thus, the resulting electron system is not truly one-dimensional. The width and shape of the electronic spectra of such a system depend not only on the confining potentials but also on electron motion in the y-direction. To illustrate the influence of these factors and for comparison with experiment, we use a simple model in which the confinement between two steps is described by a hard wall on the upper side of one step and a delta function barrier, $V_{\alpha}\delta$, at the lower side. We then calculate the probability density at the middle of the terrace as a function of energy for a 1D system (x only) and a 2D system (x and y) at both T = 0 K and 300 K. Results for a 36-Å-wide terrace and parameters corresponding to the surface state of Au(111) are shown in Figure 15. The strong dependence

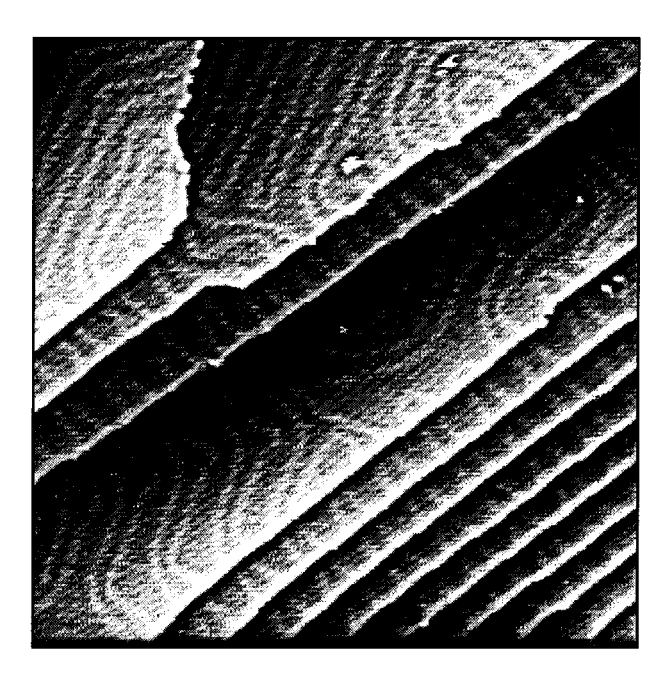
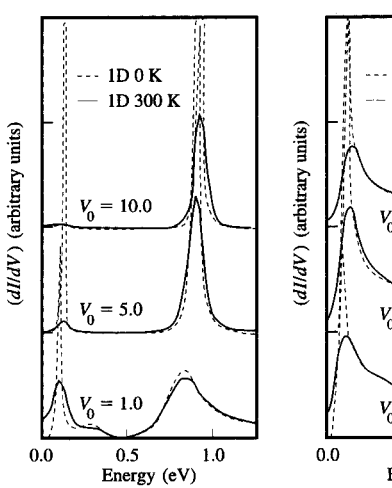
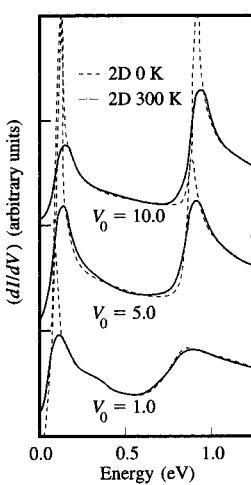


Figure 12

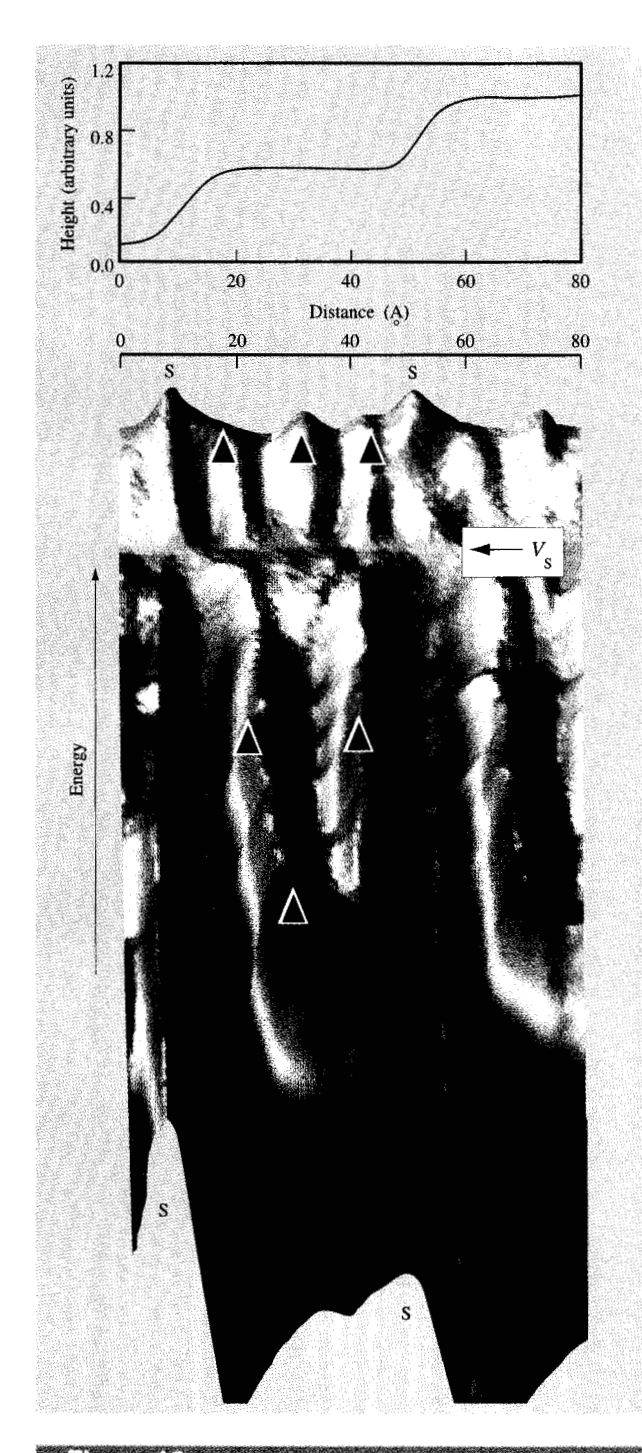
STM image of a stepped 85×85 -nm² Au(111) surface. The sample bias is +0.23 V. The pairs of lines seen on the terraces are due to the $22 \times \sqrt{3}$ reconstruction of the Au(111) surface. From Reference [22], reproduced with permission; © 1994 American Association for the Advancement of Science.





Falle 15

Simulations of the spectra of confined electron states of a 36-Å-wide terrace as a function of the confining barrier V_0 in (a) one and (b) two dimensions (see text). Dashed lines and solid lines give results at 0 K and 300 K, respectively. The electron effective mass was taken to be that of the surface state of Au(111) $(m^* = 0.28)$.



Top: STM line scan across a narrow (36-Å) terrace of a stepped Au(111) surface. Bottom: Probability density distribution of the confined electron states of this terrace at 300 K. This is a 3D map of dI/dV (\propto LDOS) as a function of the distance perpendicular to the steps, and of the sample voltage, which varies from -0.47 V (bottom) to +0.38 V (top). Step-edge structures are marked by S. The stabilization voltage is +0.23 V. From Reference [22], reproduced with permission; © 1994 American Association for the Advancement of Science.

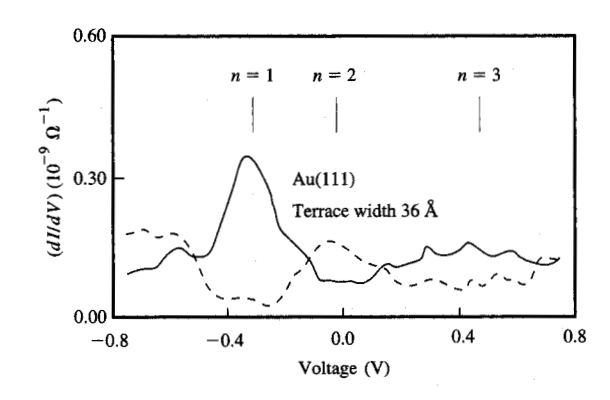


Figure 17

Tunneling spectra of the confined states of a 36-Å-wide Au(111) terrace. The solid line gives the spectrum obtained with the tip placed over the center of the terrace, while the dotted line gives the spectrum with the tip placed at a distance equal to a quarter of the terrace width from the step edge. From Reference [22], reproduced with permission; © 1994 American Association for the Advancement of Science.

of the spectral shapes, widths, and intensities on the confining barrier height and on dimensionality is clearly evident. The spectra taken at the middle of the terrace show only the odd, n=1, 3 states, while the n=2 state appears weakly only when the difference between the confining potentials is large. Most significantly, the 2D system is seen to exhibit a quasi-1D electronic behavior analogous to that seen in quantum wires. The asymmetric character of the spectra results from the fact that 1D DOS in the y-direction decreases with increasing energy $\left[\propto \left(E_0-E\right)^{-1/2}\right]$. As we see below, the calculated spectrum for a 2D system with $V_0=1$ eVÅ is in rough agreement with experimental results.

In Figure 16 we show experimental evidence of confinement at a 36-Å-wide Au(111) terrace at 300 K. This is a 3D plot of the probability density ($\propto dI/dV$) of the confined states of the terrace, as a function of the distance perpendicular to the step and of the electron energy, which increases from bottom to top. In the blue area at the bottom of the figure, the energy is lower than the onset of the surface-state band. The structure seen in this case is due to the electronic structure of the steps (marked S), and to the corrugation due to the $22 \times \sqrt{3}$ reconstruction of the Au(111) surface. After crossing into the surface band, we observe the probability distribution of the nodeless n = 1 standing-wave state formed between the two steps; this then changes into the distribution of the n = 2 state (one node), and finally we observe the distribution of the n = 3 state (two nodes). The gradual evolution is due to the broadening produced by the unconstrained motion in

the direction parallel to the steps, the low confining barriers, and finite temperature.

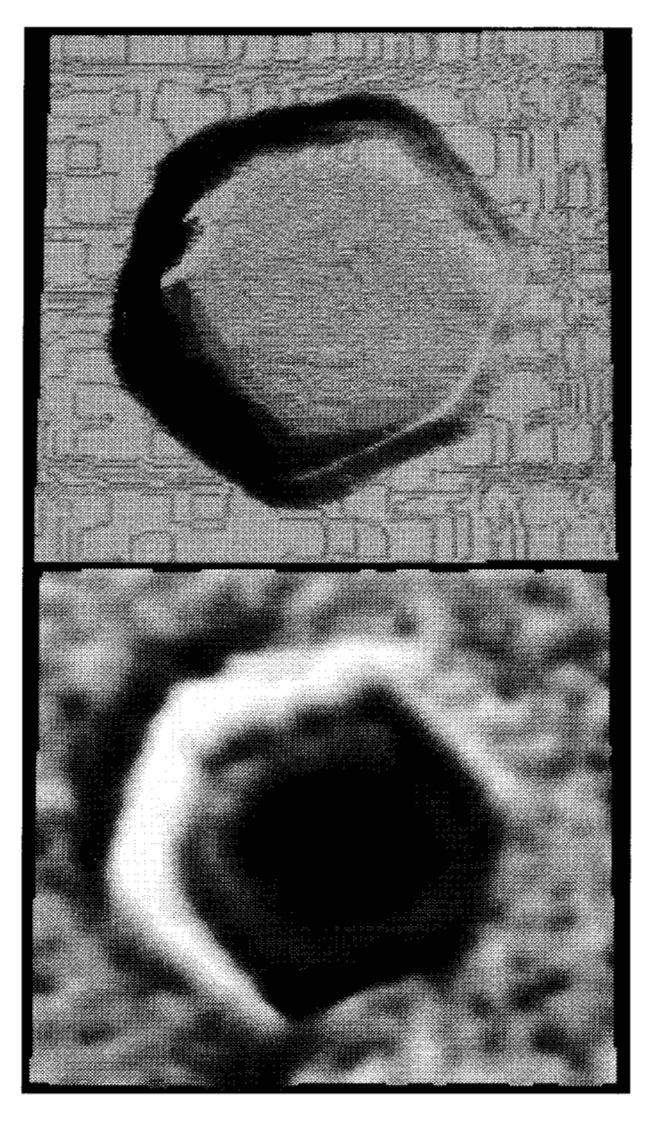
The formation of confined states at the narrow terrace is also reflected in the discrete character of its spectra. Figure 17 shows the tunneling spectra of the terrace. As we saw in the simulations in Figure 15, the tunneling spectra are position-dependent. Because there is an approximate center of symmetry, only odd quantum number states are observed with the tip positioned at the center of the terrace (even n states have a node at the center).

Finally, in **Figure 18** we illustrate 0D-electron confinement in a small silver island. Figure 18 (top) shows an STM topograph of the island ("radius" $\sim 45 \text{ Å}$), while Figure 18 (bottom) gives a dI/dV image obtained at $\sim 0.1 \text{ eV}$ above the onset of the surface-state band of Ag(111). While the STM topograph does not reveal any structure on the surface of the island, the spectral image shows a clear standing-wave pattern encompassing the island. This wave pattern can be properly accounted for by considering a superposition of the probability distributions of two overlapping box states [22].

4. Summary/conclusions

In conclusion, we have demonstrated two new applications of the STM. First, we utilized tip-sample point contacts to search for electrical transport through the dangling-bond surface state of Si(111)-7×7. The non-ohmic character and large spreading resistance of these nanocontacts, in conjunction with chemical quenching experiments, allowed us to prove the existence of such a transport channel. We also demonstrated that the electrical properties of individual nanostructures can be probed using tip-sample point contacts.

In the second part of the paper, we showed that the interaction of surface-state electrons of metals with individual surface features such as a step or an adsorbate can be studied using the STM. Electron scattering by these features leads to electron interference and the production of an oscillatory local density of states which is readily imaged in STM spectroscopic maps. Analysis of such maps for Au(111) and Ag(111) surfaces provides novel information on the electron-scattering processes involved. Surface steps were found to act as barriers for surfacestate electrons. This property was used to confine them and to form quasi-1D and 0D structures. Quasi-1D behavior is exhibited by terraces with widths of the order of the surface Fermi wavelength, while 0D behavior is found in metallic islands of similar radius. The spatial distributions of the probability density of the confined states were imaged, and their discrete spectra were obtained.



Halling II.

Top: 8.2×8.2 -nm² STM image of a Ag island. Bottom: Spectroscopic image of the same island at a sample bias of -0.01 V. From Reference [22], reproduced with permission; © 1994 American Association for the Advancement of Science.

References

- G. Binnig, H. Rohrer, Ch. Gerber, and E. Weibel, *Phys. Rev. Lett.* 49, 571 (1982).
- Scanning Tunneling Microscopy, Vols. I, II, and III, H. J. Gutherodt and R. Wiesendanger, Eds., Springer-Verlag, Berlin, 1992; Scanning Tunneling Microscopy, J. A. Stroscio and W. J. Kaiser, Eds., Academic Press, Inc., Boston, 1993.
- K. Takayanagi, Y. Tanishiro, M. Takahashi, and S. Takahashi, J. Vac. Sci. Technol. A 3, 1502 (1985).
- D. E. Eastman, F. J. Himpsel, J. A. Knapp, and K. C. Pandey, *Physics of Semiconductors*, B. L. H. Wilson, Ed., Institute of Physics, Bristol, 1978, p. 1059.

- F. J. Himpsel and Th. Fauster, J. Vac. Sci. Technol. A 2, 815 (1984)
- R. J. Hamers, R. M. Tromp, and J. E. Demuth, *Phys. Rev. Lett.* 56, 1972 (1986).
- M. Henzler, in Surface Physics of Materials, Vol. 1, Academic Press, Inc., New York, 1975, and personal communication (Y. H.).
- B. N. J. Persson and J. E. Demuth, *Phys. Rev. B* 30, 5968 (1984);
 B. N. J. Persson, *Phys. Rev. B* 34, 5916 (1986).
- S. D. Kevan and R. H. Gaylord, Phys. Rev. B 36, 5809 (1987).
- L. C. Davis, M. P. Everson, R. C. Jaklevic, and W. Shen, Phys. Rev. B 43, 3821 (1991).
- (a) Y. Hasegawa and Ph. Avouris, *Phys. Rev. Lett.* 71, 1071 (1993);
 (b) Ph. Avouris, I.-W. Lyo, R. Walkup, and Y. Hasegawa, *J. Vac. Sci. Technol. B* 12, 1447 (1994).
- M. F. Crommie, C. P. Lutz, and D. M. Eigler, *Nature* 363, 524 (1993).
- 13. Ph. Avouris and R. Wolkow, Phys. Rev. B 39, 5071 (1989).
- R. Landauer, IBM J. Res. Develop. 1, 223 (1957); J. Phys. Condens. Matter 1, 8099 (1989).
- S. M. Sze, Physics of Semiconductor Devices, 2nd ed., Wiley, New York, 1981.
- Ph. Avouris, I.-W. Lyo, and Y. Hasegawa, J. Vac. Sci. Technol. A 11, 1725 (1993).
- F. J. Himpsel, G. Hollinger, and R. A. Pollack, *Phys. Rev. B* 28, 7014 (1983).
- T. Ando, A. B. Fowler, and F. Stern, Rev. Mod. Phys. 54, 437 (1984).
- J. J. Harris, J. A. Pals, and R. Woltjer, Rep. Prog. Phys. 52, 1217 (1989).
- 20. Ph. Avouris, Solid State Commun. 92, 11 (1994).
- J. Friedel, Adv. Phys. 3, 446 (1954); J. de Physique et le Radium 17, 27 (1956).
- 22. Ph. Avouris and I.-W. Lyo, Science 264, 942 (1994).
- E. J. Heller, M. F. Crommie, C. P. Lutz, and D. M. Eigler, *Nature* 369, 464 (1994).
- Ph. Avouris, I.-W. Lyo, and P. Molinas-Mata, in Electronic Surface and Interface States on Metallic Systems, E. Bertel and M. Donath, Eds., World Scientific Press, Singapore, 1995.
- 25. Y. Hasegawa and Ph. Avouris, Science 258, 1763 (1992).
- Ph. Avouris, I.-W. Lyo, and P. Molinas-Mata, Chem. Phys. Lett. 240, 423 (1995).
- G. Leschik, R. Courths, and H. Wern, Surf. Sci. 294, 355 (1993).
- See for example H. Roder, E. Hahn, H. Brune, J.-P. Bucher, and K. Kern, *Nature* 366, 141 (1993).
- M. F. Crommie, C. P. Lutz, and D. M. Eigler, Science 262, 2181 (1993).

Received October 17, 1994; accepted for publication July 18, 1995

Phaedon Avouris IBM Research Division, Thomas J. Watson Research Center, P.O. Box 218, Yorktown Heights, New York 10598 (AVOURIS at YKTVMV, avouris@watson.ibm.com). Dr. Avouris is a member of the research staff in the Physical Sciences Department of the Thomas J. Watson Research Center. He received his B.S. degree in physical chemistry from Michigan State University in 1975. After postdoctoral work at the University of California, Los Angeles, and AT&T Bell Laboratories, he joined IBM in 1978. From 1984 to 1993 he was manager of chemical physics at the Thomas J. Watson Research Center. His research involves studies of the electronic structure and chemistry of semiconductor and metal surfaces, and nanofabrication. In recent years Dr. Avouris has concentrated on atomic-scale modification and manipulation of materials using the scanning tunneling microscope. He received two IBM Outstanding Technical Achievement Awards for his work in this area. Dr. Avouris has published 200 technical papers and edited a book. He is a fellow of the American Physical Society.

In-Whan Lyo IBM Research Division, Thomas J. Watson Research Center, P.O. Box 218, Yorktown Heights, New York 10598 (LYO at YKTVMV, lyo@watson.ibm.com). Dr. Lyo received a B.S. degree in physics from Seoul National University in 1980, and a Ph.D. degree in physics from the University of Pennsylvania in 1988 for his study of electronic structures in metals using angle-resolved photoemission. Since then, he has worked in the Physical Sciences Department at the Thomas J. Watson Research Center, first as a postdoctoral fellow and later as an advisory engineer, studying surfaces of semiconductors and metals using STM. In 1993, he received an Outstanding Technical Achievement Award for his work on manipulation of strongly bound atoms with the STM. Dr. Lyo is a member of the American Physical Society.

Yukio Hasegawa Institute for Materials Research, Tohoku University, 2-1-1, Katahira, Aoba-ku, Sendai 980-77, Japan (hasegawa@apfim.imr.tohoku.ac.jp). Dr. Hasegawa is an associate professor at the Institute for Materials Research at Tohoku University, Japan. He received B.S., M.S., and Ph.D. degrees, all in applied physics, from the University of Tokyo in 1985, 1988, and 1991. His Ph.D. thesis was on studies of semiconductor surfaces and interfaces using STM and BEEM techniques. In 1990, he worked at AT&T Bell Laboratories as a visiting researcher, joining IBM the following year as a postdoctoral fellow. From 1992 to 1994, Dr. Hasegawa was a research associate at the Mesoscopic Materials Research Center, Kyoto University. His current research interests are in nanoscale physics at surface and interface.